NUMERICAL ANALYSIS OF A CONCRETE THERMAL ENERGY STORAGE SYSTEM FOR ADIABATIC COMPRESSED AIR ENERGY STORAGE

Abdullah Masoud Ali[1],*, Audrius Bagdanavicius[1], Edward R. Barbour[2], Daniel L. Pottie[2], Seamus Garvey[3], James Rouse[3], Zahra Baniamerian[3]

[1]School of Engineering, University of Leicester, Leicester, LE1 7RH, UK

[2]Centre for Renewable Energy System Technology (CREST), Loughborough University, Loughborough, LE11 3TU, UK

[3]Faculty of Engineering, University of Nottingham, Nottingham, NG7 2RD, UK

*Corresponding Author: E-Mail: amsa7@leicester.ac.uk

ABSTRACT

Adiabatic Compressed Air Energy Storage (ACAES) is one of the most promising solutions to balance energy supply and demand using renewable energy sources. Thermal Energy Storage (TES) system is an integral part of ACAES. In this study, a numerical analysis was conducted to investigate the simplified design of a concrete TES system with thermal oil as the Heat Transfer Fluid (HTF) using the CFD software Simcenter STAR-CCM+. The TES system consists of individual concrete elements that can be connected in series and parallel. These elements are fitted with U-shaped steel tubes with and without fins. The numerical analysis focused on concrete elements consisting of five elements connected in series. During the charging phase which lasted 3 hours the HTF inlet temperature was fixed at 423.15 K. This phase was followed by a 1-hour standby stage and a subsequent 3-hour discharging phase. The HTF inlet temperature during the discharging stage was maintained at 298.15 K. The results demonstrate that at the end of the charging phase, in the TES system with tubes with fins the HTF output temperature drops to around 367 K. The HTF output temperature in the TES system with smooth tubes without fins is higher at around 371 K. Additionally, the use of fins improves thermal performance and augments heat storage capacity within the concrete compared to the TES system with tubes without fins. The proposed scalable TES model is designed to be easily integrated into the A-CAES system.

Keywords: Thermal Energy Storage, Compressed Air Energy Storage, Concrete Heat Storage, TES design.

1 INTRODUCTION

Energy storage systems are key to ensuring a reliable energy supply. They can absorb large amounts of energy, store it in a suitable medium for a long time, and release it in a controlled manner with a specified time delay. One such medium is air, and Compressed Air Energy Storage (CAES) systems are one of several thermomechanical energy storage systems that use gaseous air. In CAES, energy is stored in the form of compressed air in tanks or underground caverns during periods of low electricity demand (off-peak) and then released during peak electricity demand to generate electricity. Depending on the type of CAES system, air can be compressed to 100 bar or more. Typically, the compression of the air takes place in several stages to avoid high temperatures, which can reach up to 500 K depending on the compression ratio of the compressor (Mitra *et al.*, 2022). The charging and discharging processes involve heat generation and heat demand phases, so Thermal Energy Storage (TES) systems should be used to improve the performance of CAES. TES systems are used to store heat or cold, and the methods of storage can be divided into physical (sensible heat or latent heat storage) or chemical processes. Sensible heat storage is the most common method of heat storage and plays an important role in all thermomechanical energy storage systems, including CAES. CAES systems can be classified according to their power output: large-scale CAES (>100 MW), medium-scale CAES (<100 MW) and micro-scale CAES (up to 10 MW) (Mitra *et al.*, 2022). Large-scale CAES systems are typically used for grid-related applications such as load shifting, peak shaving, and frequency/voltage control. On the other hand, small-scale CAES systems operate on a low-voltage grid, which provides an excellent solution to the problems associated with the use of renewable energies and enables the development of independent systems for remote communication devices. Compared to other energy storage technologies such as

https://doi.org/10.52202/077185-0081

battery energy storage or flywheel energy storage, CAES offers numerous advantages, including, an extended operational lifespan, substantial storage and release capacity (Zhang *et al.*, 2021). In traditional CAES systems, when demand is high, the stored compressed air is released, heated using a heat source from the combustion of fossil fuels, and then expanded in turbines to generate electricity. However, this approach is not sustainable. In order to improve the efficiency of CAES and reduce the dependency on fossil fuels, heat generated during the charging stage could be stored and reused later. In this case, since the heat is not removed but remains within the system, it is classified as adiabatic CAES (A-CAES). Thermal Energy Storage (TES) systems are an integral part of A-CAES. In A-CAES with TES heat is absorbed and stored during the air compressions stage, and is used to pre-heat the air prior to expansion. This efficient method of reusing the heat generated during air compression enables A-CAES to achieve higher cycle efficiencies compared to conventional CAES (Luo *et al.*, 2016).

Several researchers investigated A-CAES with TES, where indirect heating and cooling of compressed air is carried out using heat exchangers. Jannelli *et al.* (2014) used this method in a small-scale A-CAES using renewable energy power plants. It was demonstrated that the proposed configuration had the potential for indirect heating and cooling, achieving an overall A-CAES storage efficiency of 57%, calculated as the ratio of the electricity produced by the turbines to the electricity consumed by the compressors. Zhang *et al.* (2021) investigated the integration of small-scale A-CAES with wind turbines. They reported that TES increases flexibility and addresses variable electricity demand. They demonstrated that up to 88% energy efficiency can be achieved. However, in other investigations smaller efficiency of CAES was reported. For example, in a study by Sciacovelli *et al.* (2017) an efficiency of 70% was obtained.

TES systems, which are an essential part of the A-CAES, can be divided into systems with physical processes (sensible or latent heat storage) or chemical processes. Sensible TES systems made from concrete provide a simple and economical solution compared to other TES systems (Cabeza et al., 2022). The cost of high-temperature concrete in a solid TES system is around 0.08 €/kg and 3 €/ kWh, making it the most economical option compared to molten salt and castable ceramics (Navarro *et al.*, 2012). Concrete is widely available and produced using well-established processes, with high mechanical strength. Concrete has a specific heat between 0.7 and 0.82 kJ/kg K and a thermal conductivity between 0.5 and 2.21W/m K (Xu and Chung, 2000, Doretti *et al.*, 2019). Furthermore, TES with concrete can reduce the environmental impact when compared to phase change material (PCM) or molten salt energy storage systems (Miró et al., 2016). Concrete TES systems were examined in various applications, such as in solar power plants (Laing et al. (2009) and Salomoni et al. (2014)). According to these studies, concrete is a highly desirable heat storage material.

Numerous studies investigated methods how to increase the amount of energy transferred to the TES during the charging phase by increasing the temperature in the TES. One effective solution was the implementation of fins to extend heat transfer surfaces. Various fin designs are used, such as radial and longitudinal fins, which are attached to the outer surface of the pipe.

Several studies, such as Rathod and Banerjee (2015), have experimentally investigated the impact of three longitudinal fins on the thermal performance of shell and tube Latent Heat Thermal Energy Storage (LHTES) systems. Their results indicate that the use of three longitudinal fins leads to a 12.5% reduction in melting compared to the scenario without fins. Dekhil *et al.* (2022) considered eight configurations, four of which had 4, 8, 16, and 32 longitudinal fins, while the remaining four had 4, 8, 16, and 32 radial fins in LHTES. They examined the impact of fin redistribution while maintaining a constant total heat transfer surface. Among these configurations, the use of 4 longitudinal fins resulted in the most significant heat transfer enhancement due to the shortest melting/solidification process time compared to other fin arrangements. Based on these findings, it can be inferred that longitudinal fin design is characterised by reliable performance, ease of manufacture and cost-effectiveness.

This study examines a concrete TES system which is used to store heat during the charging phase and subsequently release it during the discharging phase in a small or medium-scale A-CAES system with indirect heating and cooling. The proposed TES design can be fully scaled up or down by adding or removing elements that can be connected in series or parallel. This research aims to analyse how to improve the heat transfer between Heat Transfer Fluid (HTF) and concrete and how to control the temperature of the HTF during charging or discharging phases. Also the effect of standby phase on the discharging phase is investigated.

https://doi.org/10.52202/077185-0081

The TES system consists of many concrete elements that could be connected in series or in parallel. These elements are fitted with U-shaped steel pipes. Thermal oil is used as HTF and circulates in the pipes. This numerical analysis is used for five elements connected in series. During the 3-hour charging phase, the inlet HTF temperature is held constant at 423.15 K. This phase was succeeded by a 1-hour standby stage, followed by a subsequent 3-hour discharging phase with the inlet HTF temperature maintained at constant 298.15 K.

2 METHODOLOGY

2.1 Operation of A-CAES

The layout of a simplified small or medium-scale A-CAES combined with the TES system, investigated in this study, is shown in Figure 1. The system operates in three phases: charging, discharging and standby. In the charging stage, also known as the compression stage, the compressor compresses the air (solid lines), which passes through the heat exchanger (HEX). The hot compressed air is then cooled in the heat exchanger by the HTF (thermal oil Paratherm NF) and is stored in the tank or underground cavern at high pressure and low temperature. During the discharging phase, the cold compressed air (dotted lines) is released from the storage, preheated in the HEX, and then expands in the turbine, which is connected to the generator.

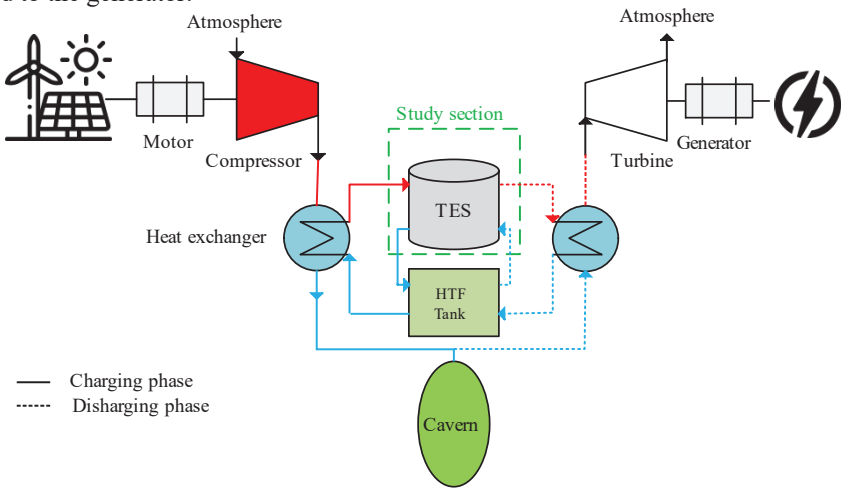

Figure 1: Schematic of the A-CAES combined with TES. Solid lines represent the charging phase and dotted lines represent the discharging phase.

2.2 Thermal Energy Storage (TES) system

A TES system constructed of concrete is used to store the heat extracted from the HTF as it leaves the HEX. The HTF circulates between the HEX, TES, and HTF tank. During the charging phase, the HTF is supplied from the oil tank to the HEX and then to the TES (solid lines), where heat is transferred from the HTF to the concrete, charging the TES. The primary objective of this system is to effectively decrease the temperature of the hot air before it is supplied to the air storage tank or underground cavern. During the discharging phase, the HTF is supplied from the tank to the TES (dotted lines), where it is heated. The hot HTF is then pumped to the HEX, where the air, released from the tank or cavern, is preheated before expanding in the turbine. The primary focus of this stage is to ensure that the temperature of the HTF remains adequately high, thereby ensuring the temperature of the air is as high as possible. Throughout this process, it is assumed that the mass flow rate of the HTF remains constant. The choice of concrete for this TES system is based on its properties, availability and cost-effectiveness. The TES system used in this study consists of 5 elements connected in series. The system could be expanded by adding more elements in series and in parallel. An example of a TES system consisting of 5 elements connected in series and arranged in a 5x10 grid is depicted in Figure 2 (a). Thanks to this design, the entire TES takes up little space. Stacking the elements either vertically or horizontally results in a better surface-to-volume ratio, thus reducing heat loss, especially in larger systems. It also facilitates production and transport processes before on-site installation. The proposed design is scalable and can meet a wide range of TES capacity requirements. The TES system consists of individual concrete elements connected in series and parallel. These elements are fitted with U-shaped steel tubes with and

https://doi.org/10.52202/077185-0081

without longitudinal fins. In this study, the objective of the numerical analysis was to analyse a concrete column consisting of five elements connected in series (Figure 2(b)). Paratherm NF thermal oil was selected as HTF. The dimensions of the analysed TES are shown in Table 1. Table 2 shows the thermo-physical properties of concrete, carbon steel and Paratherm NF oil.

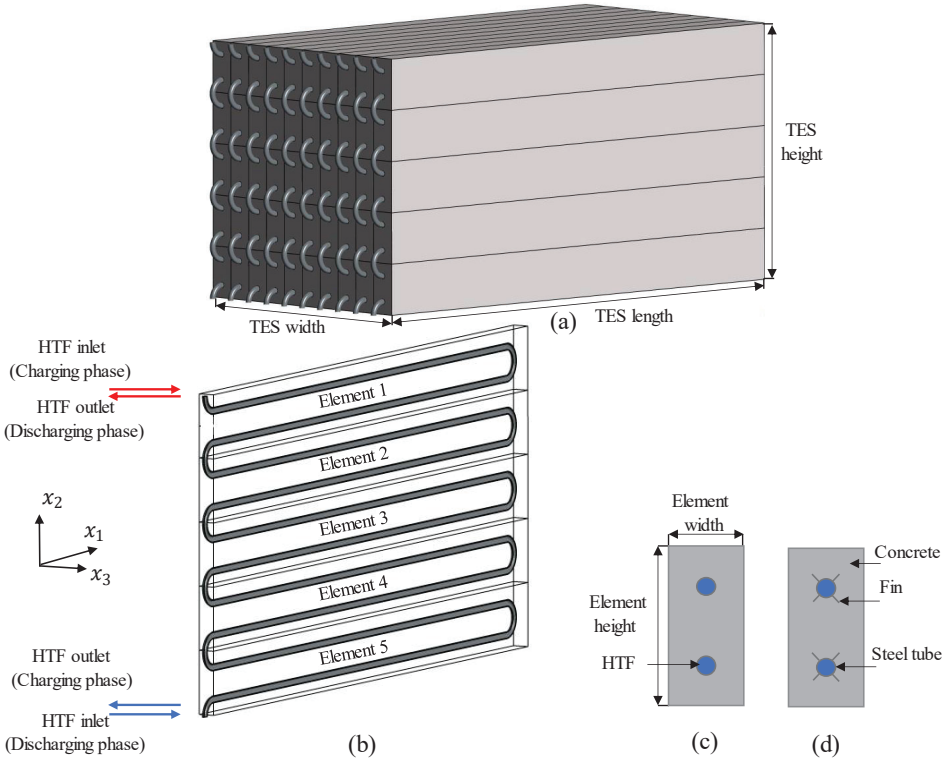

Figure 2: (a) Isometric view of the TES, (b) isometric view of the investigated configuration of five elements connected in series, (c) front view of one element, (d) front view of one element with fins.

Table 1: Geometric dimensions of the TES, in mm

Specification	Values
TES height	1500
TES width	1500
TES length	3000
Element height	300
Element width	150
Element length	3000
Inner pipe diameter	26.6
Outer pipe diameter	33.4
Fin height	60
Fin thickness	3.4

Table 2: The thermo-physical properties of concrete (Doretti *et al.*, 2019), carbon steel and Paratherm NF oil (temperatures in °C) (Fluids, 2009).

	Concrete	**Carbon steel**	**Paratherm NF oil**
Density ρ (kg/m^3)	2483.0	7832	-0.651T+895.6
Specific heat C_P (J/kg · K)	820.0	434	8.0593e-5T^3-0.036T^2+9.699T+1603.66
Thermal conductivity k (W/m · K)	2.21	63.9	1.124e-24T^3-2.99e-22T^2-8e-5T+0.1098
Kinematic viscosity μ (N · s/m^2)	-	-	-2.987e-8T^3+1.035e-5T^2-0.0012T+0.05

https://doi.org/10.52202/077185-0081

2.3 Mathematical formulation

The aim of numerical analysis was to analyse one column of TES consisting of five concrete elements connected in series (Figure 2 (b)). Each of these elements has a U-shaped tube designed to circulate HTF Paratherm NF oil. In this study, conjugate heat transfer approach was used. Using this approach the energy equation is solved simultaneously for fluid domain and solid domain. It is assumed that the heat flux between fluid and solid is conserved and equation (1) could be used (Pater *et al.*, 2023).

$$\dot{q}_f + \dot{q}_s = 0 \tag{1}$$

Where $\dot{q}_f$ is the heat flux from the fluid boundary and $\dot{q}_s$ is the heat flux through the solid boundary. The governing equation for energy transport within a solid domin (HTF tube and concrete) is captured by the heat conduction equation (3) (Ouyang *et al.*, 2017, Ali *et al.*, 2021).

$$\rho_s \, Cp_s \frac{\partial T_s}{\partial t} = \nabla \cdot (k_s \nabla T_s) \tag{2}$$

where ρ is density, Cp is heat capacity, k is thermal conductivity and T is temperature.

The Laplace equation is coupled using the time-averaged Navier-Stokes equations that describe the behavior of the HTF. The numerical solution involves solving the continuity, momentum and energy equations of the HTF, subject to certain assumptions:

1. The HTF flow is three-dimensional, laminar, incompressible and Newtonian, with temperature dependence and mass flow given at the inlet.
2. The radiative heat transfer is not involved.
3. The thermal properties of the concrete and steel tube are assumed constant.

The governing equations for HTF are (Ali *et al.*, 2022a, Ali *et al.*, 2022b):

$$\nabla \cdot \vec{u}_{HTF} = 0 \tag{3}$$

$$\rho_{HTF} \frac{\partial \vec{u}}{\partial_t} + \nabla \cdot (\rho_{HTF} \vec{u}_i \vec{u}_i) = -\nabla p_{HTF} + \mu_{HTF} \nabla^2 \vec{u}_{HTF} + \rho_{HTF} \vec{g} \tag{4}$$

$$\frac{\partial T_{HTF}}{\partial_t} + \rho_{HTF} \vec{u}_{HTF} \cdot \nabla T_{HTF} = \nabla \cdot (k_{HTF} \nabla T_{HTF}) \tag{5}$$

The variables used to describe the properties and boundaries of the HTF include viscosity μ, velocity vector $\vec{u}$, absolute pressure p and gravitational acceleration in the negative x_2 direction $\vec{g}$, here x_2 signifies the axial direction, as shown in Figure 2. At the interface between solid and solid domains (HTF tube and concrete), the heat transfer equation can be expressed using equation (6).

$$-k_{HTF\ tube} \frac{\partial T_{HTF\ tube}}{\partial x_n} = -k_{Concrete} \frac{\partial T_{Concrete}}{\partial x_n} \tag{6}$$

where, n represents the normal coordinate to the walls.

2.4 Numerical solver

In this study, a three-dimensional model was explored. The process commenced with the geometric design in ANSYS Design Modeler, followed by mesh generation using ANSYS Meshing. Subsequently, the model was implemented in the computational fluid dynamics software Simcenter STAR-CCM+, and the results were visualized using Tecplot 360 CFD post-processing tool. Three different regions were identified in the model: HTF, steel and concrete. The simulations were conducted using an implicit unsteady solver with a second-order temporal discretization solver for segregated flow and segregated energy equations. These equations addressed mass, momentum, and energy conservation within the fluid domain, which was modelled as a laminar flow. The boundary conditions were defined as follows: the inlet was defined as a mass flow inlet with a constant total temperature method. The outlet boundary is a pressure outlet with a static pressure of 0 Pa (gauge). The front, back, top, and bottom faces of the five elements were modeled as adiabatic. The right and left faces of the five elements were modeled as "symmetry". Interfaces were meticulously established between elements and between the elements and the solid tube. These interfaces were modelled as an internal interface

https://doi.org/10.52202/077185-0081

with "In-place Topology" for fluid-tube interactions and as a contact interface with "In-place Topology" for fluid-solid interactions. In-place interface topology in STAR-CCM+ is a method used to create interfaces between different regions or parts of a computational domain. In STAR-CCM+, the "In-Place Interface Topology" is used to connect fluid and solid domains for Conjugate Heat Transfer or solid and solid domains for modeling thermal and mechanical interactions (Siemens, 2024). The computational cost for physical time of 3 hours charging, 1 hour standby and 3 hours discharging was approximately 60 hours of wall clock, using 64 cores performed on a 2.4 GHz shared memory high-performance computer cluster.

2.5 Boundary conditions

In order to assess the impact of the TES design on the charging, standby and discharging processes, our analysis takes into account the 3-hour charging, 1-hour standby and 3-hour discharging phases. It was assumed that the flow of the HTF is laminar with Re number between ~1200 for charging stage and ~300 for discharging stage and the mass flow rate was constant 0.05 kg/s. Table 3 shows all parameters utilised in all three phases.

Table 3: The boundary conditions of the proposed TES.

Parameter	Charging	Standby	Discharging
Time (hour)	3	1	3
Mass flow rate (kg/s)	0.05	0	0.05
$T_{f,in}$ (K)	423.15	-	298.15
$T_{initial}$ (K)	298.15	-	-

2.6 Grid independence and time step test

The evaluation of prediction of sensitivity of the computational domain was conducted by analyzing the TES. This investigation involved a stepwise refinement of a coarse mesh until reaching a point where the average concrete temperature values demonstrated significant stability regardless of further mesh refinement. Figure 3 (a) illustrates the average concrete temperature of the TES without fins during the charging phase, across five different grid sizes: 2, 4, 10, 14 and 18 million. The inlet HTF temperature was held constant at 423.15 K and the mass flow rate was 0.05 kg/s. Notably, the figure reveals no substantial alteration in the average concrete temperature as the number of elements exceeds 14 and 18 million. Consequently, a mesh size comprising 14 million cells was deemed adequate for modelling in this study. Figure 3 (b) shows the relationship between the average concrete temperature and time across four different time steps: 16, 8, 4, and 2 s. It can be concluded that there is no significant difference between the 4 and 2 s time steps, therefore 4 s timestep is used in this study.

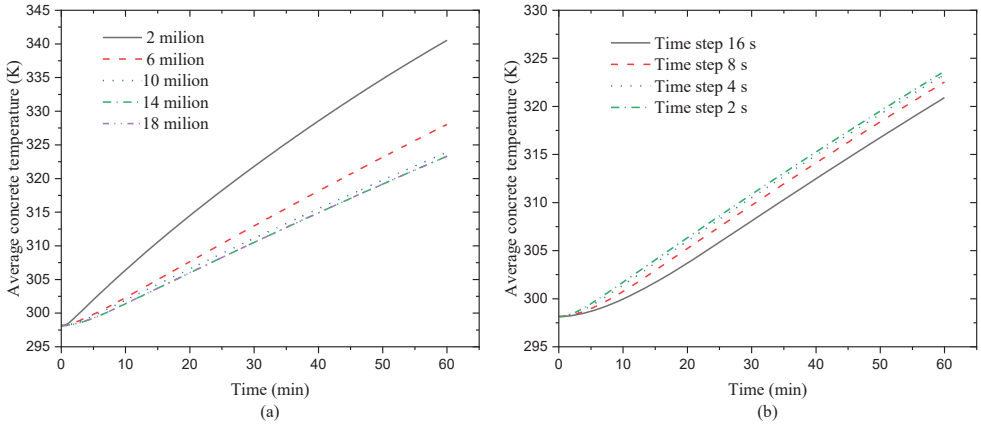

Figure 3: (a) Grid independence test results of the average concrete temperature across the TES without fins during the charging phase of five different grid sizes: 2, 4, 10, 14 and 18 million and (b) Time step test results of the average concrete temperature across four different time steps of 16, 8, 4, and 2 s.

https://doi.org/10.52202/077185-0081

2.7 Validation

To evaluate the numerical models, the numerical results of the Paratherm NF (HTF) outlet temperature and the average concrete temperature during the charging phase are compared with the experimental results conducted by Doretti *et al.* (2019) ((a) (b) **Figure 4**). The concrete element used is a stainless steel AISI 316 tube embedded into the concrete in four passages. The concrete element has a length of 3m, while the HTF tube has an inner diameter of 14 mm and an outer diameter of 16 mm, with a total tube length of 12 m. The inlet HTF temperature was 324 K, and the mass flow rate was 0.12 kg/s. The predictions of the HTF output temperature and the average concrete temperature are in good agreement with the experimental results. These results enable the use of the model with confidence for the current study.

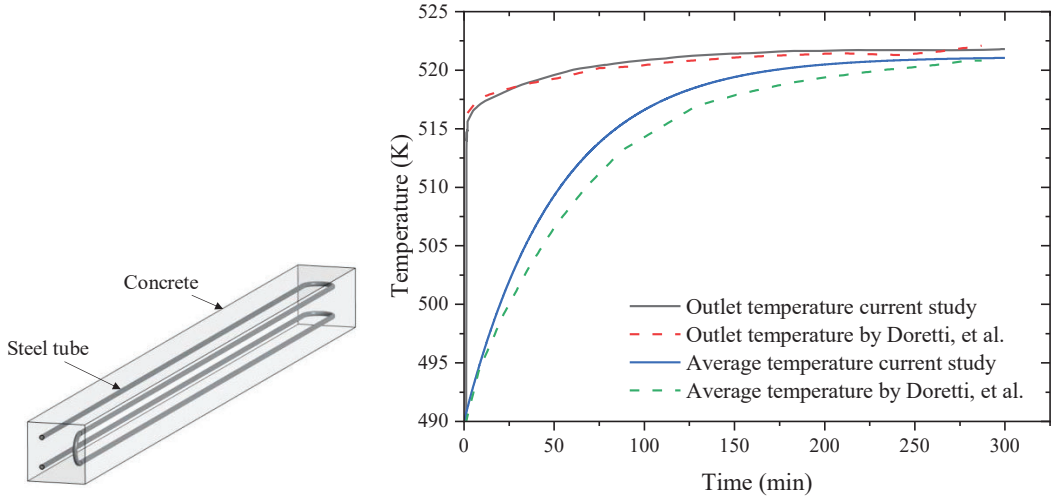

(a) (b)

Figure 4: (a) Isometric view of a concrete element by Doretti *et al.* (2019) and (b) Validation of numerical results of the outlet HTF temperature and the average concrete temperature against experimental results conducted by Doretti *et al.* (2019).

3 RESULTS AND DISCUSSION

3.1 Temperature distribution in TES

In Figure 5, the temperature distribution is shown for TES with smooth tubes and for TES with tubes with fins at the end of the 3 hours charging phase (a), 1-hour standby phase (b), and 3 hours discharging phase (c), in the x_1= 1.5 m and x_3= 0 m planes. The temperature distribution is displayed using an iso-level color scheme, where blue represents 298.15 K and red indicates 423.15 K. Figure 5 (a) shows that the HTF temperature reduces from 423.15 K (in red) at the TES inlet to 371.48 K (in light green) at the TES exit, and that the highest temperature is obtained it the top element. Other elements that are closer to the outlet have lower temperatures. Using fins the HTF temperature reduces from 423.15 K (in red) at the TES inlet to 367.8 K (light green) at the outlet. Figure 5 (b) shows the temperature distribution after the standby phase. During the stand-by phase, the mass flow rate is set to 0 kg/s, and the HTF remains in the tubes. The HTF temperature decreases as a result of the heat transfer from the high-temperature regions in the HTF and the steel tube to the concrete. During the discharging phase, the flow is reversed, and the HTF enters at the point that was the exit of the TES during the charging stage, with a temperature of 298.15 K. Figure 5 (c) shows that, due to the use of fins, the HTF temperature increases monotonically from 298.15 K (in blue) at the inlet to 330.4 K (in light blue) at the outlet.

https://doi.org/10.52202/077185-0081

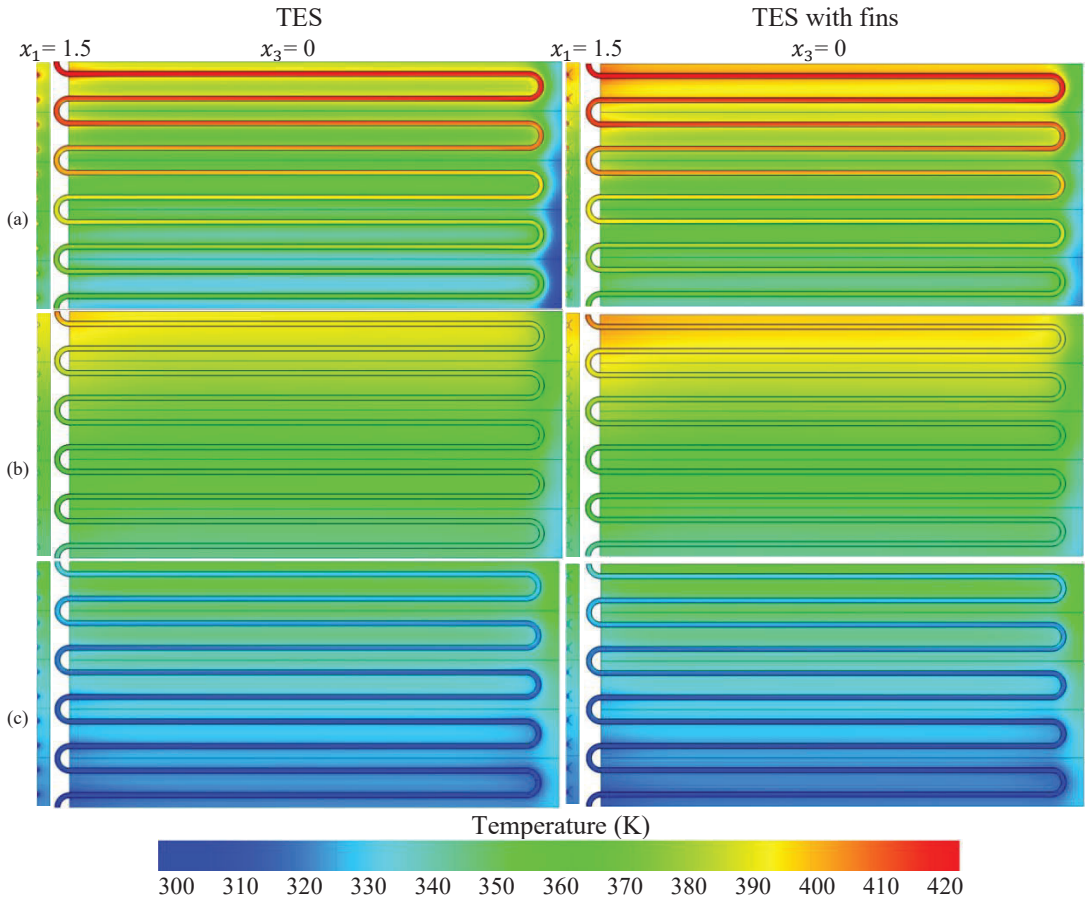

Figure 5: Temperature distributions of the five elements in x_1= 1.5 m plane and x_3= 0 m plane after charging (a), standby (b) and discharging (c) phases.

3.2 The thermal characteristics of the TES

The HTF output temperature significantly impacts the thermal performance of the TES. It is particularly important to ensure suitable HTF temperatures when the TES is integrated into a CAES. In the charging phase, the lowest outlet temperature of the HTF and the highest temperature of the TES is desirable, which means that the TES stores more heat. The temperature of TES also directly affects the working fluid temperature that will be used during the discharging phase. Figure 6 shows the HTF outlet and inlet temperatures for each element during the charging, standby and discharging phases of the TES. Figure 6 (a) shows the HTF outlet temperatures for all elements of the TES with smooth tubes. It is observed from this figure that the HTF temperature difference between the inlet (inlet temperature ~ 423 K) and outlet (~ 320 K for element 5) is initially high at the beginning of the charging process, but then this difference decreases significantly and the outlet temperature after the fifth element reaches ~ 370 K at the end of the process. This demonstrates the effectiveness of using five elements connected in series, which leads to an increase in the heat transfer rate between the HTF and the concrete while decreasing the HTF temperature after each element. The proposed modular design of the TES allows more than five elements to be connected in series, further reducing the HTF temperature after each element during the charging phase. During the standby phase, the HTF is not flowing, resulting in a decrease in its temperature due to heat transfer from the HTF and the steel tube to the concrete. During the standby phase, heat is more evenly distributed among the concrete elements (Figure 5 (b)). At the beginning of the discharging phase (Figure 6), when the flow of HTF in the TES is reversed, a sharp reduction in the HTF outlet temperature is observed. The outlet temperature in the last element (black

https://doi.org/10.52202/077185-0081

bold line represents HTF outlet temperature for element 1 during the discharging phase) suddenly drops to ~360 K and then gradually reduces to approximately ~330 K.

Figure 6 (b) shows the HTF outlet and inlet temperatures for each element of the TES with tubes with fins during the charging, standby and discharging phases. The addition of fins helps in decreasing the HTF outlet temperature in the charging phase, enabling better heat storage within the TES. At the end of charging phase, the HTF outlet temperature for TES with fins is 3.8 K lower than that of the TES with smooth tubes at the same conditions. On the other hand, in the discharging phase, these fins contribute to a rise in the HTF outlet temperature, enhancing the efficiency of TES thermal storage. At the end of discharging phase, the HTF outlet temperature for TES with fins is 2.2 K higher than of the TES without fins at the same conditions. These results demonstrate that small modifications, such as the addition of fins and an increase in the heat transfer area, have only a minor impact on the temperature of the HTF. However, the modular design allows the TES to be expanded according to the size of the system and other requirements.

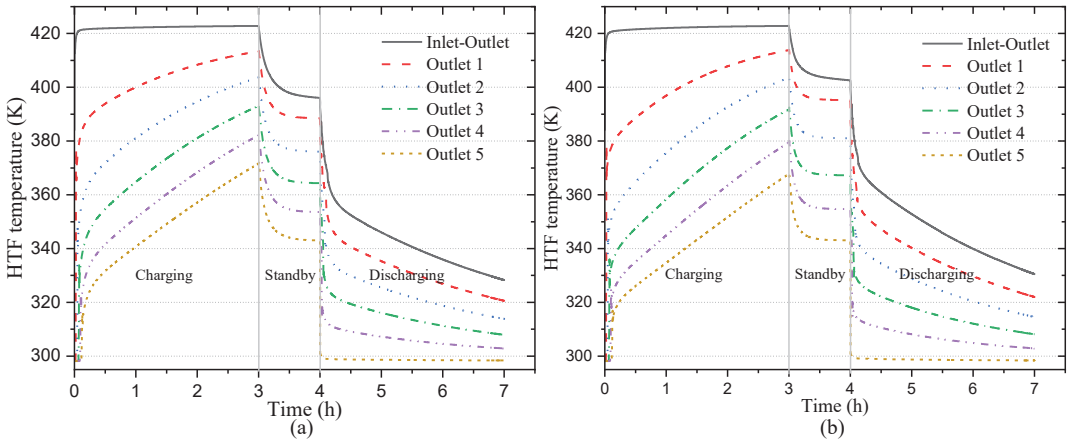

Figure 6: HTF temperature at the outlet of the element during the charging, standby and discharging phases for a mass flow rate of 0.05 kg/s. (a) TES with smooth tubes; (b) TES with tubes with fins

Figure 7 shows the concrete temperature for each element and the average temperature of the TES during the charging, standby and discharging phases. The average concrete temperature is calculated by integrating the temperature over the concrete volume and dividing it by the total concrete volume. It is evident that the concrete temperature for all elements and the average TES temperature (bold line) increase over time as more heat is transferred during the charging phase. The use of fins helps to accelerate the heat transfer from the HTF to the concrete. These fins extend the surface area of the outer HTF tube, enhancing heat transfer efficiency, enabling effective heat dissipation from the HTF tube, and promoting a more uniform temperature distribution, as shown in Figure 5 (a). At the end of the charging phase, the average concrete temperature for TES with fins is 3.4 K higher than of the TES without fins. The average concrete temperature remains relatively constant during the standby phase. During the discharging phase the average concrete temperature decreases due to heat transfer from the concrete to the HTF. Fins also contribute to accelerating heat transfer in the discharging phase by absorbing more heat from the concrete and transferring it to the tube, which then transfers it to the HTF. At the end of discharging phase, the average concrete temperature for TES with fins is 0.7 K lower than that of the TES without fins under the same conditions.

https://doi.org/10.52202/077185-0081

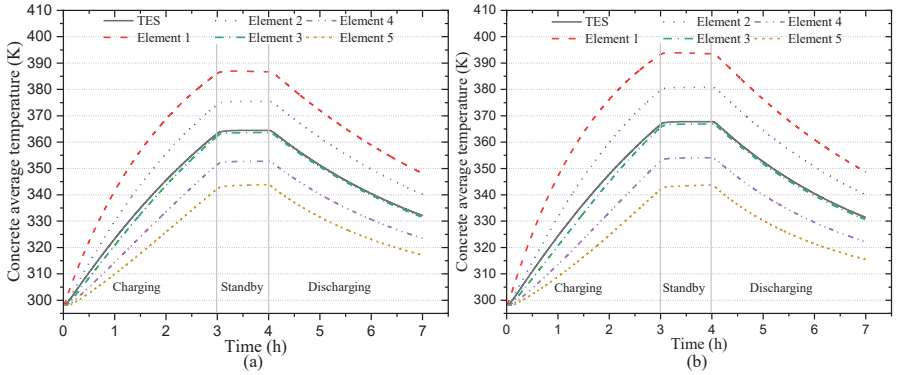

Figure 7: Comparison of average concrete temperature for (a) TES with smooth tubes and (b) TES with fins during the charging, standby and discharging phases for a mass flow rate of 0.05 kg/s.

3.3 The energy stored in the TES

Figure 8 shows the specific energy of the TES with smooth tubes (a) and in the TES with fins (b) during the charging, standby and discharging phases. The specific energy is a function of temperature; therefore, it follows the temperature change pattern. The average specific energy stored is calculated by integrating the specific energy over the concrete volume and dividing it by the total concrete volume. During the charging phase the specific energy increases and remains almost constant during the standby phase. During the discharge phase, the specific energy decreases but does not reach the initial values observed at the start of the charging phase.

In the TES with fins, a noticeable upward shift of the average curve (bold line) is observed, similar to the temperature change, indicating an enhanced charging rate. However, the impact of fins on the specific energy is not very significant. Comparing Figure 6 and Figure 8 reveals that while the addition of fins leads to only a modest change in the HTF temperature, there is a more observable increase in the amount of energy stored in the TES. At the end of the charging phase, the specific energy for the TES with fins is 3.4 kJ/kg higher than that for the TES without fins.

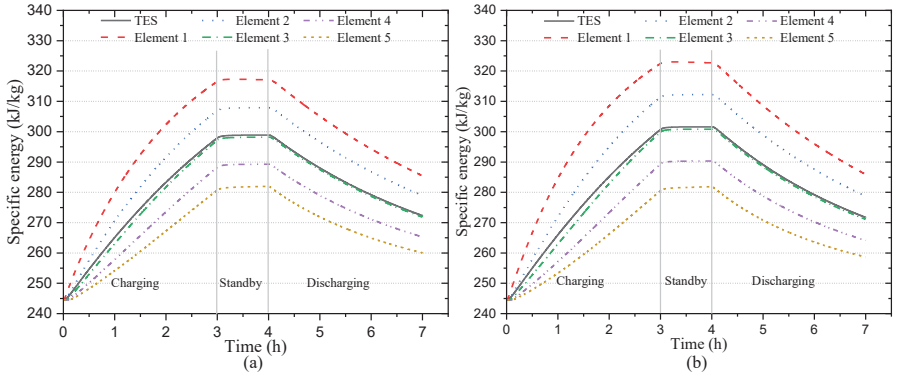

Figure 8 Comparison of specific energy stored for (a) TES with smooth tubes and (b) TES with fins during the charging, standby and discharging phases for a mass flow rate of 0.05 kg/s.

4 CONCLUSIONS

This work identified and assessed the thermal performance of the Thermal Energy Storage (TES) system integrated with the small or medium scale Adiabatic Compressed Air Energy Storage (A-CAES) system. In this study, a numerical analysis was conducted to investigate the simplified design of a concrete TES system with thermal oil as the Heat Transfer Fluid with a constant mass flow rate. The concrete TES consisting of a column of five concrete blocks connected in series with smooth tubes and with tubes with fins was investigated during the 3-hour charging, 1-hour standby, and 3-hour discharging phases.

It was observed that during the charging phase the HTF temperature difference between the inlet and outlet is initially high at the beginning, and then this difference gradually decreases with time. During

https://doi.org/10.52202/077185-0081

the standby phase, the HTF is not flowing, and its temperature decreases due to the heat transfer from high temperature regions in the HTF and steel tube to the concrete. During the discharging phase there is a sharp temperature drop of the HTF outlet temperature and then the HTF outlet temperature gradually decreases. The study shows that the use of concrete elements connected in series is clearly beneficial for controlling the outlet temperature of the HTF.

The use of small fins aids in decreasing the HTF outlet temperature during the charging phase, enabling slightly better heat storage within the TES. At the end of this phase, the HTF outlet temperature for TES with fins is slightly lower than that of the TES without fins under the same conditions. During the discharging phase, these fins contribute to a rise in the HTF outlet temperature, enhancing the efficiency of TES thermal storage, higher HTF outlet temperature for TES with fins is observed compared to the TES without fins at the same conditions. The benefit of using fins, compared to a configuration without fins, is suggested to result from an extension in the HTF tube's outer surface area. This increase enhances heat transfer between the HTF and the concrete, leading to a lower temperature difference between the HTF flow and tube wall during the charging phase. However, small modifications like adding fins have a minor effect on the HTF outlet temperature. The use of fins also has a minimal impact on both the average temperature of the TES and the specific energy of the TES. Therefore, further research is necessary to investigate potential methods for improving heat transfer in concrete TES.

One of the objectives of this study was to analyse a modular TES consisting of several elements connected in series. This design enables the use of less space in the construction of the TES and improves the surface-to-volume ratio. The TES can be scaled up or down to meet different heat capacity requirements. The individual elements of the TES can be stacked on top of each other, allowing for a reduction of thermal losses, particularly in large-scale systems. These stacked elements can be connected in series to reduce the HTF temperature or in parallel to increase the heat capacity of TES.

This study shows the importance of controlling the HTF output temperature at different stages of TES operation, emphasising the effectiveness of the configuration when small elements are connected in series. The temperature change trends observed during the charge, standby and discharge phases provide valuable insights into optimising the thermal performance of TES, especially when integrated with CAES systems. Valuable information is also provided for the modeling and simulation of A-CAES systems integrated with TES or for the design and analysis of TES as stand-alone systems.

NOMENCLATURE

Symbols

Cp	Specific heat	J/kg
$\vec{g}$	gravitational acceleration	(m/s^2)
K	Thermal conductivity	W/(m·K)
p	Pressure	Pa
$\dot{q}$	Heat flux	W/m^2
T	Temperature	K
u	Fluid velocity	m/s

Greek symbols

μ	Viscosity	kg/(m·s)
ρ	Density	kg/m^3

Abbreviations

CAES	Compressed Air Energy Storage
HEX	Heat Exchanger
HTF	Heat Transfer Fluid
LHTES	Latent Heat Thermal Energy Storage
PCM	Phase Change Material
TES	Thermal Energy Storage

REFERENCES

Ali, A. M., Angelino, M. Rona, A. 2022a. Physically consistent implementation of the mixture model for modelling nanofluid conjugate heat transfer in minichannel heat sinks. *Appl. Sci.,* 12**,** 7011.

Ali, A. M., Rona, A. Angelino, M. 2022b. Numerical investigation of various twisted tapes enhancing a circular microchannel heat sink performance. *Int. J. Heat Fluid Flow,* 98**,** 109065.

https://doi.org/10.52202/077185-0081

Ali, A. M., Rona, A., Kadhim, H. T., Angelino, M. Gao, S. 2021. Thermo-hydraulic performance of a circular microchannel heat sink using swirl flow and nanofluid. *Appl. Therm. Eng.,* 191.

Cabeza, L. F., Vérez, D., Zsembinszki, G., Borri, E. Prieto, C. 2022. Key challenges for high temperature thermal energy storage in concrete—first steps towards a novel storage design. *Energies,* 15**,** 4544.

Dekhil, M. A., Simo Tala, J. V., Bulliard-Sauret, O. Bougeard, D. 2022. Numerical analysis of the effect of the iso-surface fin redistribution on the performance enhancement of a shell-and-tube latent heat thermal energy storage unit for low-temperature applications. *J. Energy Storage,* 56**,** 105892.

Doretti, L., Martelletto, F. Mancin, S. 2019. A simplified analytical approach for concrete sensible thermal energy storages simulation. *J. Energy Storage,* 22**,** 68-79.

Fluids, P. H. T. 2009. Paratherm™ HE Thermal Properties [Online]. Available: https://www.paratherm.com/heat-transfer-fluids/paratherm-he-htf/ [Accessed 04/01/2024].

Jannelli, E., Minutillo, M., Lubrano Lavadera, A. Falcucci, G. 2014. A small-scale CAES (compressed air energy storage) system for stand-alone renewable energy power plant for a radio base station: A sizing-design methodology. *Energy,* 78**,** 313-322.

Laing, D., Lehmann, D., Fiß, M. Bahl, C. 2009. Test Results of Concrete Thermal Energy Storage for Parabolic Trough Power Plants. *J. Sol. Energy Eng.,* 131.

Luo, X., Wang, J., Krupke, C., Wang, Y., Sheng, Y., Li, J., Xu, Y., Wang, D., Miao, S. Chen, H. 2016. Modelling study, efficiency analysis and optimisation of large-scale Adiabatic Compressed Air Energy Storage systems with low-temperature thermal storage. *Appl. Energy,* 162**,** 589-600.

Miró, L., Gasia, J. Cabeza, L. F. 2016. Thermal energy storage (TES) for industrial waste heat (IWH) recovery: A review. *Appl. Energy,* 179**,** 284-301.

Mitra, S., Mahato, A. C., Nag, A. Kumar, D. 2022. Various methodologies to improve the energy efficiency of a compressed air energy storage system. *Energy Storage,* 4**,** e315.

Navarro, M. E., Martínez, M., Gil, A., Fernández, A. I., Cabeza, L. F., Olives, R. Py, X. 2012. Selection and characterization of recycled materials for sensible thermal energy storage. *Solar Energy Materials and Solar Cells,* 107**,** 131-135.

Ouyang, X.-L., Xu, R.-N. Jiang, P.-X. 2017. Three-equation local thermal non-equilibrium model for transient heat transfer in porous media: The internal thermal conduction effect in the solid phase. *Int. J. Heat Mass Transf.,* 115**,** 1113-1124.

Pater, M., Kaaks, B., Lauritzen, B. Lathouwers, D. 2023. A numerical benchmark for modelling phase change in molten salt reactors. *Annals of Nuclear Energy,* 194**,** 110093.

Rathod, M. K. Banerjee, J. 2015. Thermal performance enhancement of shell and tube Latent Heat Storage Unit using longitudinal fins. *Appl. Therm. Eng.,* 75**,** 1084-1092.

Salomoni, V. A., Majorana, C. E., Giannuzzi, G. M., Miliozzi, A., Di Maggio, R., Girardi, F., Mele, D. Lucentini, M. 2014. Thermal storage of sensible heat using concrete modules in solar power plants. *Solar Energy,* 103**,** 303-315.

Sciacovelli, A., Li, Y., Chen, H., Wu, Y., Wang, J., Garvey, S. Ding, Y. 2017. Dynamic simulation of Adiabatic Compressed Air Energy Storage (A-CAES) plant with integrated thermal storage – Link between components performance and plant performance. *Appl. Energy,* 185**,** 16-28.

Siemens.2024. Simcenter STAR-CCM+ Documentation. Siemens Digital Industries Software. Available: https://plm.sw.siemens.com/en-US/simcenter/fluids-thermal-simulation/star-ccm/ [16/05/2024].

Xu, Y. Chung, D. D. L. 2000. Cement of high specific heat and high thermal conductivity, obtained by using silane and silica fume as admixtures. *Cement and Concrete Research,* 30**,** 1175-1178.

Zhang, X., Qin, C., Xu, Y., Li, W., Zhou, X., Li, R., Huang, Y. Chen, H. 2021. Integration of small-scale compressed air energy storage with wind generation for flexible household power supply. *J. Energy Storage,* 37**,** 102430.

ACKNOWLEDGEMENT

This research was supported by the EPSRC award "Sustainable, Affordable and Viable Compressed Air Energy Storage" (SAVE-CAES, EP/W027569/1. This research used the ALICE High Performance Computing Facility at the University of Leicester.

https://doi.org/10.52202/077185-0081